Hindawi Publishing Corporation
New Journal of Science
Volume 2014, Article ID 524042, 9 pages
http://dx.doi.org/10.1155/2014/524042

Research Article

Biomimetic-Inspired Infrared Sensors from Zn_3P_2 Microwires: Study of Their Photoconductivity and Infrared Spectrum Properties

M. Israelowitz,[1] B. Weyand,[2] C. Leiterer,[3] V. Munoz,[4] C. Martinez-Tomas,[4] M. Herraiz-Llacer,[4] I. Slowik,[3] C. Beleites,[3] W. Fritzsche,[3] C. Krafft,[3] T. Henkel,[3] M. Reuter,[5] S. W. H. Rizvi,[1] C. Gille,[1] K. Reimers,[3] P. M. Vogt,[2] and H. P. von Schroeder[1,6]

[1] *Biomimetics Technologies Inc., Toronto, ON, Canada M6S 2X4*
[2] *Hannover Medical School, Department of Plastic, Hand and Reconstructive Surgery, 30625 Hannover, Germany*
[3] *Leibniz Institute of Photonic Technology, Albert-Einstein-Straße 9, 07745 Jena, Germany*
[4] *Department of Applied Physics and Electromagnetism, University of Valencia, 46100 Valencia, Spain*
[5] *The Technical University of Clausthal-Zellefeld, Julius Albert Straße 4, 38678 Clausthal-Zellerfeld, Germany*
[6] *University of Toronto, Toronto Western Hospital, East Wing 2nd Floor, 399 Bathurst Street, Toronto, ON, Canada M5T 2S8*

Correspondence should be addressed to H. P. von Schroeder; herb.vonschroeder@uhn.ca

Received 1 April 2014; Revised 18 May 2014; Accepted 18 May 2014; Published 26 June 2014

Academic Editor: Rakez Kayed

The fire beetle, *Melanophila acuminata* (Coleoptera: Buprestidae), senses infrared radiation at wavelengths of 3 and 10–25 microns *via* specialized protein-containing sensilla. Although the protein denatures outside of a biological system, this detection mechanism has inspired our bottom-up approach to produce single zinc phosphide microwires *via* vapour transport for IR sensing. The Zn_3P_2 microwires were immobilized and electrical contact was made by dielectrophoresis. Photoconductivity measurements have been extended to the near IR range, spanning the Zn_3P_2 band gaps. Purity and integrity of the Zn_3P_2 microwires including infrared light scattering properties were confirmed by infrared transmission microscopy. This biomimetic microwire shows promise for infrared chip development.

1. Introduction

Nature has provided certain species, such as snakes [1] and insects, with specific sensors for light detection in the infrared range [2–5]. The black fire beetle, *Melanophila acuminata*, is one of those insects which possess a pair of natural infrared detectors [6]. The position and composition of the infrared sensors in *M. acuminata,* which are shown in Figures 1(a), 1(b), and 1(c), have been extensively studied by us and other groups [7, 8]. In our recent work we found that the tulip-shaped protein region within each sensillum with its lipid borders is highly sensitive for infrared radiation at wavelengths around 3 μm and between 10 and 25 μm [8]. In order to use a biomimetic approach to transfer this intriguing idea from nature into modern technical applications such as an infrared microchip, several points need to be considered.

Firstly, the unique composition and structure of the natural infrared sensor have to be transferred into a practical technical application. Secondly, natural elements of the sensor may require artificial substitutes with specific optoelectronic properties. Since proteins outside of their biological system begin to denature (a process in which the folding structure of a protein is altered due to exposure to certain chemical or physical factors causing the protein to become biologically inactive), durable synthetic alternatives are required [9, 10]. Das et al. were able to integrate a bacterial reaction center and a plant photosystem, the spinach chloroplast, into a solar cell of organic semiconductor system in order to convert

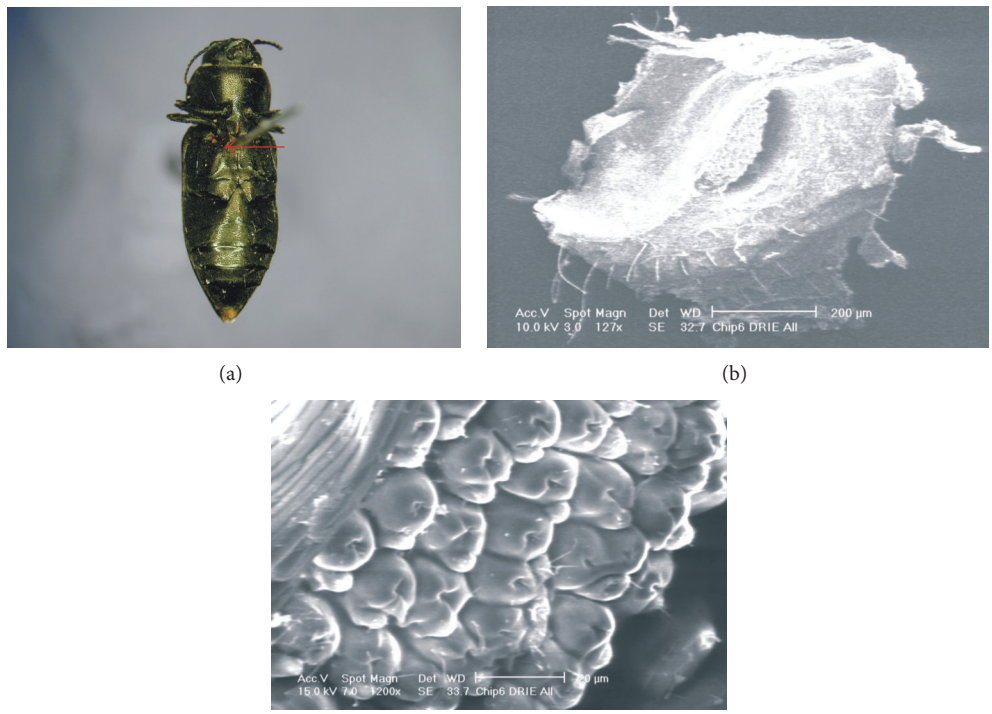

(a) (b) (c)

Figure 1: (a) Photograph of the underside of the fire chaser beetle *M. acuminata* showing one of the two infrared sensory pits (red circle and arrow) by which the beetle detects and is attracted to forest fires across large distances. (b) Scanning electron micrograph of one *M. acuminata* sensory pit with 150 sensilla and (c) showing each sensillum having a top dimple used to filter wavelengths (with permission by Elsevier).

light into electricity, but the proteins denatured within two weeks [11]. In order to avoid problems due to the biological denaturation process, inorganic semiconductor materials with photoconductive activity in the infrared range must be considered (in our case Zn_3P_2) [12]. Our experience with different semiconductors has led us to testing zinc phosphide for this potential application.

Any detector, whether it is synthetic or organic, must also overcome thermal noise [13]. The thermal noise is the difference between the source and the background [14]. As photons reaching a detector are not distributed uniformly in energy and frequency, it is difficult to screen the signal [15] especially for the middle and far infrared bands unless the system temperature is exceptionally cooled, between 77 and 100 Kelvin [16].

Infrared absorbance characteristics of bulk zinc phosphide have been previously investigated and documented for the spectral range between 400 cm^{-1} and 3800 cm^{-1} and for the far infrared range between 45 cm^{-1} and 400 cm^{-1} [17, 18]. Band patterns can be observed only in the far infrared region whereas the spectrum in the infrared region remains unstructured. Starting with an absorbance of 0.1 at 400 cm^{-1}, the absorbance continually increases with increasing wavenumbers, reaching a value of 1 at approximately 3000 cm^{-1}. Further investigations of the hh- (heavy holes-) and lh- (light holes-) bands have been reported [19–22]. Initial studies on photoconductivity of single Zn_3P_2 microwires have been reported by Wu et al. [23] for the UV/VIS excitation wavelengths between 325 nm and 633 nm. In this study a top-down approach using a sequence of photolithography steps, metal deposition, and lift-off processes was utilized for wiring the Zn_3P_2 nanowire in an electrode gap, formed by two gold electrodes. Another setup has been made by Yu et al. [24] using lithograph-assembled arrays of Zn_3P_2 nanowires on silicon and PET substrates. On the other hand, dielectrophoresis has been reported as an approach for the immobilization of individual silicon nanowires between electrodes to study their optical properties [23, 25, 26].

In contrast to the top-down process, described by Wu et al. [23] and Yu et al. [24], the purpose of this project was to develop an efficient bottom-up approach based on dielectrophoresis for placement and contacting of individual microwire in the electrode gap. The advantage of this technique is that it allows for the selective preparation of a single microwire bridge. Moreover, multiple electrode gaps on a single chip can be processed in parallel potentially allowing the cost efficient and reliable preparation of nanowire sensor arrays for camera and sensing applications.

2. Materials

2.1. Melanophila acuminata. Adult *M. acuminata* were provided by Richard Westcott (Entomologist Emeritus, Oregon Department of Agriculture, Salem, USA) and Nathan Schiff

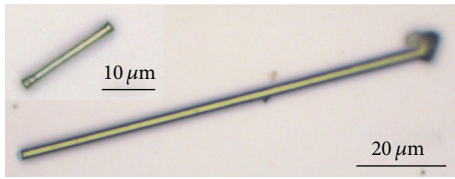

Figure 2: Zinc phosphide needles used to measure light in the infrared spectrum. The geometry is added to measure the absorption.

(US Forest Service, Southern Research Station, Stoneville, Mississippi, USA). Specimens were collected at the Sandy River delta near Portland and Ollalie Lake, Cascade Range, elevation 1615 m, both in Oregon, United States. The beetles were kept at 25°C in humidified environment.

2.2. Zinc Phosphide. After optimization of growth conditions, single needles of zinc phosphide (Zn_3P_2) (Figure 2) were grown by physical vapour transport [27, 28] in a two-zone furnace. Powder Zn_3P_2 (Sigma Aldrich) was used as the source material for needle growth. The material was sealed under vacuum (<1 Pa) in quartz ampoules in which the growth took place. The ampoules were carbon coated by cracking of methane at 1000°C in order to avoid chemical reaction between the Zn_3P_2 and the silica and prevent oxidation.

3. Method

3.1. Scanning Electromicroscopy. The SEM micrographs of *M. acuminata* sensillawere taken with an electron microscope Philips XL 30 XL FEG SEM. The sensilla samples were treated with ethanol to remove the lipid in the cuticular region.

3.2. Dielectrophoresis. Dielectrophoresis characterizes the motion of dielectric objects in an alternating electrical field [29] and throughout the years has been proven to be valuable technique for the manipulation of micro- and nanosized objects [30–32]. In our case, dielectrophoretic manipulation of zinc phosphide was performed in a methanol solution using an alternating electrical field (sinusoidal) between two gold microelectrodes.

The microelectrodes were set *via* photolithography providing gap widths in the lower micrometer range.

3.3. Infrared Spectroscopy. Fourier transform infrared spectroscopy (FTIR) [33, 34] was used to characterize the absorption properties of the Zn_3P_2 microwires. Infrared spectra of KBr tablets were acquired with an IFS 66 FT-IR spectrometer (Bruker/Germany). Ca. 0.6 mg Zn_3P_2 microwires were ground with approximately 200 mg KBr and pressed into a clear 12 mm KBr tablet; 128 coadditions at 4 cm^{-1} resolution were recorded between 400 cm^{-1} and 6000 cm^{-1}.

FTIR-images of individual Zn_3P_2 microwires were collected in the spectral range from 1000 cm^{-1} to 5000 cm^{-1} in transmission mode using a Varian 670 (Agilent, USA) FT-IR spectrometer equipped with a 64 × 64 pixel focal plane array (FPA) detector and a 15x Cassegrain objective. The nominal pixel size of this system is 5.6 μm. 64 scans of an empty CaF_2 slide (background) and 32 scans of the microwires on the same CaF_2 slide were coadded and the FTIR spectra were analysed in R [35], using packages hyperSpec [36] for the spectroscopic data and ggplot2 [37] for graphical display.

4. Zn_3P_2 Characteristics

Zn_3P_2 is a p-type material with a band gap of about 1.4 eV, near the optimum for use in photovoltaic conversion of solar energy [38]. Recently, theoretical band structure curves for zinc phosphide have been calculated, including effects of crystal field splitting of the valence band [39].

Zn_3P_2 has an anion sublattice in close proximity to the standard FCC (face centered cubic) packing [40]. Their cations occupy only three quarters of the tetrahedral emptiness among anions [41, 42] and the cation sublattices are exactly one-quarter vacant. These vacancies determine some key features of zinc phosphide as the presence of numerous discrete levels inside the band gap. The interaction between excitons and such deep defect levels allow for exciton recombination and/or the creation of multiple-exciton complexes. Reduction of system dimensionality, as that of zinc phosphide, sharply intensifies these effects.

A theoretical model for the band structure of a crystalline solid is given by the Kronig-Penney formulation. This formulation gives an analytically solvable model that visualizes the effect of the periodic potential on the dispersion relation of the electrons, that is, the formation of a band structure characterized by the existing band gaps. Additionally, for many semiconductors the temperature dependence of the band gaps can be described with the empirical, three-parameter Varshni formula [43–45].

From this model McQuarrie [46] provides an expression for the band structure of a crystalline solid with a one-dimensional periodic structure of the type:

$$V(x) = V_0, \quad -b < x < 0,$$
$$V(x) = 0, \quad 0 < x < a. \tag{1}$$

The energy-allowed values fall into continuous regions separated by gaps and are a function of both the relative energy of the electron in respect to the eight of the potential well $\varepsilon = E/qV_0$ and the relative width of the well ($r = b/a$). A simple model that allows an easy development of this model can be seen with a plot of the energy against the wavenumber k showing the band gaps that appear in a crystalline solid [45]. Table 1 gives the allowed values of ε for each band ($b/a = 0.20$).

5. Results

Zinc phosphide crystals were produced as linear microwires or as lambda-shaped arrangements of two linear microwires. Photoconductivity was analysed for linear microwires. Lambda-shaped arrangements were subject to infrared

Table 1: Allowed values of $\varepsilon = E/qV_0$ for a periodic potential described by (1) with the value $r = b/a = 0.20$ (taken from [46]).

Band	Range of ε
1	0.0616 to 0.0074
2	0.2425 to 0.2965
3	0.5325 to 0.6652
4	0.9192 to 1.1776
5	1.3980 to 1.8305
6	1.9791 to 2.6190
7	2.6850

Table 2: Typical geometry values and characteristics of the used of Zn_3P_2.

Property	Value
Nanowire diameter	1.9 μm
Nanowire length	85 μm
Gap width	40 μm
Metal film height	100 nm
Metal film material	Gold

spectroscopy in order to include both linear and lambda junctions in the assessment of the spectral properties. The geometric values of the experimental device are given in Table 2. The linear branches of zinc phosphide microwires were placed in the gap between two gold contacts. The chip substrate consisted of several tapered electrodes; therefore, the gap width varied from 1 μm to 40 μm in the centre of the chip. In order to measure the photoresponse, the microwire sample was trapped and fixed between two electrodes and subsequently illuminated with white light (halogen lamp ~120 Watts). When exposed to white light, the zinc phosphide microwire gives a photocurrent higher than 100 nA depending on the light flow and time; without illumination, the current was more than one order of magnitude lower than when exposed. Figure 3(a) shows this response as a function of time, where response times are less than 1 second.

For the investigation of the photocurrent as a function of the illuminating wavelength, metal interference filters were used. The resulting photoresponse measurements are shown in Figure 3(b). It can be observed that response times remain less than 1 second for all of the considered wavelengths.

The photocurrent was measured using a source of 5 V. All currents were normalized to the same surface density of the illuminated light. Figure 3(c) shows the normalized photocurrent of a single zinc phosphide (Zn_2P_3) microwire depending on the illuminating wavelength; the error bars indicated sixfold standard deviation. The optical filter characteristics for the illumination and transmission are included in Figure 3(c), normalized to 1. Kimball et al. [22] have found the direct photoconduction for Zn_2P_3 microwires to be at 827 nm and the indirect photoconduction at 898 nm [47]. In the studied region (400 nm–1200 nm), the plot of the photocurrent as a function of the excitation wavelength shows its maximum at low wavelengths and a relative maximum in the centre of the near infrared region (NIR) around 1000 nm.

Figure 3(d) shows the *I-V* characteristics of a single microwire. The *I-V* characteristics suggest a diode-like behaviour which is probably caused by Schottky barriers between the metal electrodes and the microwire. A resistance of about 400 MΩ can be derived considering the positive region.

The FTIR spectrum of Zn_2P_3 microwires ground in KBr was recorded as a tablet in the spectral region from 400 cm^{-1} to 6000 cm^{-1}. Two spectra from two tablets together with one spectrum of a pure KBr tablet (red) are shown in the lower panel of Figure 4(a). The upper panel shows the background corrected ground Zn_3P_2, obtained by manually subtracting multiples of the pure KBr spectra from the measurement in order to compensate the νCH stretching vibrations of organic impurities between 2850 cm^{-1} and 3000 cm^{-1}. Compared to the raw data, this dramatically reduced not only the νCH stretching bands, but simultaneously also the bands between 950 cm^{-1}–1200 cm^{-1} and 1380 cm^{-1}–1500 cm^{-1}, which corresponded to typical spectral regions of CH deformation vibrations and CC stretching vibrations of organic molecules. In addition the spectral signatures of water (strong broad νOH around 3450 cm^{-1}, δHOH at 1665 cm^{-1}, and a broad signal below 900 cm^{-1}) were mostly compensated for one tablet containing Zn_3P_2 and overcompensated for the other leaving a residual CO_2 signal (2350 cm^{-1} and 665 cm^{-1}). All band assignments were checked with Socrates [48].

Thus, we attribute all vibrational bands to either impurities in the KBr, water, or CO_2. The remaining unstructured absorption corresponded to the spectrum published by Nyquist et al. [17]. No additional bands, indicating, for example, the presence of phosphate (1150 cm^{-1}–1350 cm^{-1}) or ZnO (450 cm^{-1}), as possible results of the degradation of zinc-phosphide, were observed.

Individual microwires of zinc phosphide were subjected to infrared imaging in order to investigate the influence of local shape properties (linear fractions of different thickness, branches) on the infrared scattering characteristics. In contrast to the ground material, the infrared spectra of the individual zinc phosphide microwires exhibited a distinct spectral pattern dependent on the local shape of the crystal, reflecting the local light scattering properties of the crystal shape (Figure 4(d)). The observed infrared intensity (as $\log_{10} I_0 - \log_{10} I$) of the microwire as a function of the wavenumber is shown in Figure 4(d) for each location. Figure 4(b) shows the results of a principal component analysis which gives an unsupervised decomposition of the spectroscopic data set into so-called loadings (latent spectra, not shown) and scores (latent concentrations Figure 4(b)). The first principal component corresponds to the bulk Zn_3P_2 spectrum. As such, the most important part of the variation in the spectral pattern (which constituted more than 95% of the total variance) was the intensity coming from the bulk material. The higher principal components corresponded to additional varying scattering patterns. The average spectrum showed scattering in addition to the spectral signature bulk Zn_3P_2, whereas the first principal component corresponded

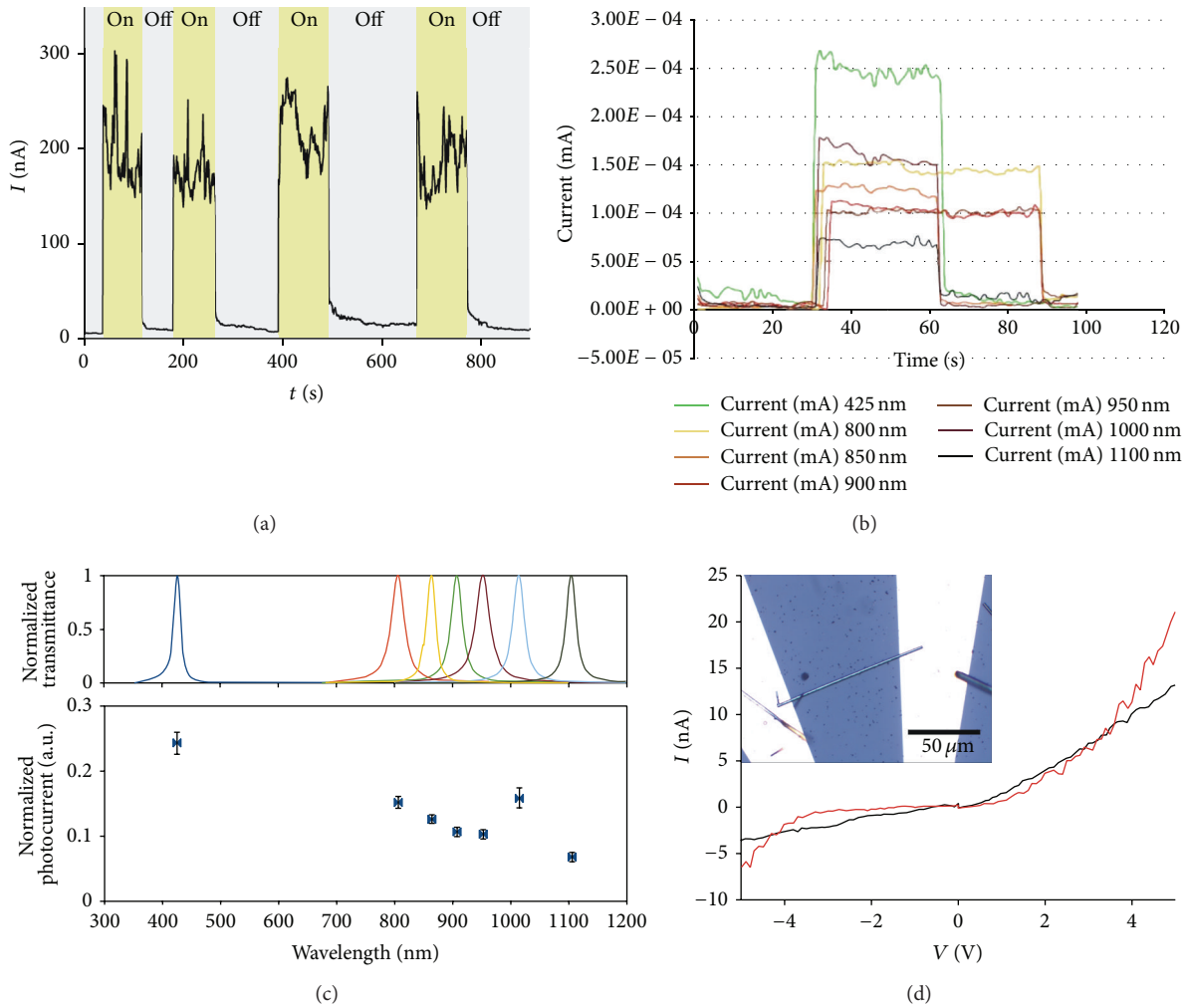

FIGURE 3: (a) Photoresponse measurements as a function of time for white light excitation. The highlighted area shows point where the light was switched on/off. KBr is hygroscopic, so already slight differences in air humidity and/or the time for handling the KBr disc and the actual measurement will lead to changes in the observed water bands. (b) The current of different wavelengths in time. (c) Photocurrent as a function of the illuminated light, normalized in respect to surface power density (given absorption efficiency), including the normalized transmission of the excitation filter characteristics from 300 nm to 1200 nm. (d) *I-V* characteristics for a linear microwire. Inset shows the device made by dielectrophoresis. The zinc phosphide wire is contacted between two metal electrodes (height: 100 nm) with a gap of ~60 μm. The known line for stability by two different measurements: the black initial is the original measurement and the red line is the measure after 7-day differences.

to the absorption spectrum, and we therefore concluded that the scattering properties (which depend on the geometry) were remarkably constant across all spectra. While a wide mix of different scattering patterns could cancel out to a shapeless loss in intensity similar to the loadings of the first principal component (also similar, though unrelated to the bulk Zn_3P_2 spectrum), such a mix of locally different scattering patterns should be accompanied by a variety of different scattering patterns across the sample which would mean that many principal components that describe scattering contributions should be observed describing a substantial amount of the total variance. This was not the case: the principal components that described scattering covered less than 5% of the observed variance in the spectra.

6. Discussion

Infrared detectors have a limitation related to the amount of signal that reaches the detector. It is beyond the quality of the detectors and is due to the fact that the photon incident to the detector and the detector itself cannot be changed or readily amplified.

This limitation can be explained from the blackbody radiation: the Stephan-Boltzmann law that gives the power radiated from a black body per unit surface in terms of its temperature. This law states that all objects above absolute zero emit radiation in the infrared part of the electromagnetic spectrum. Consequently infrared detectors have to be able to separate a signal from the background of the ambient

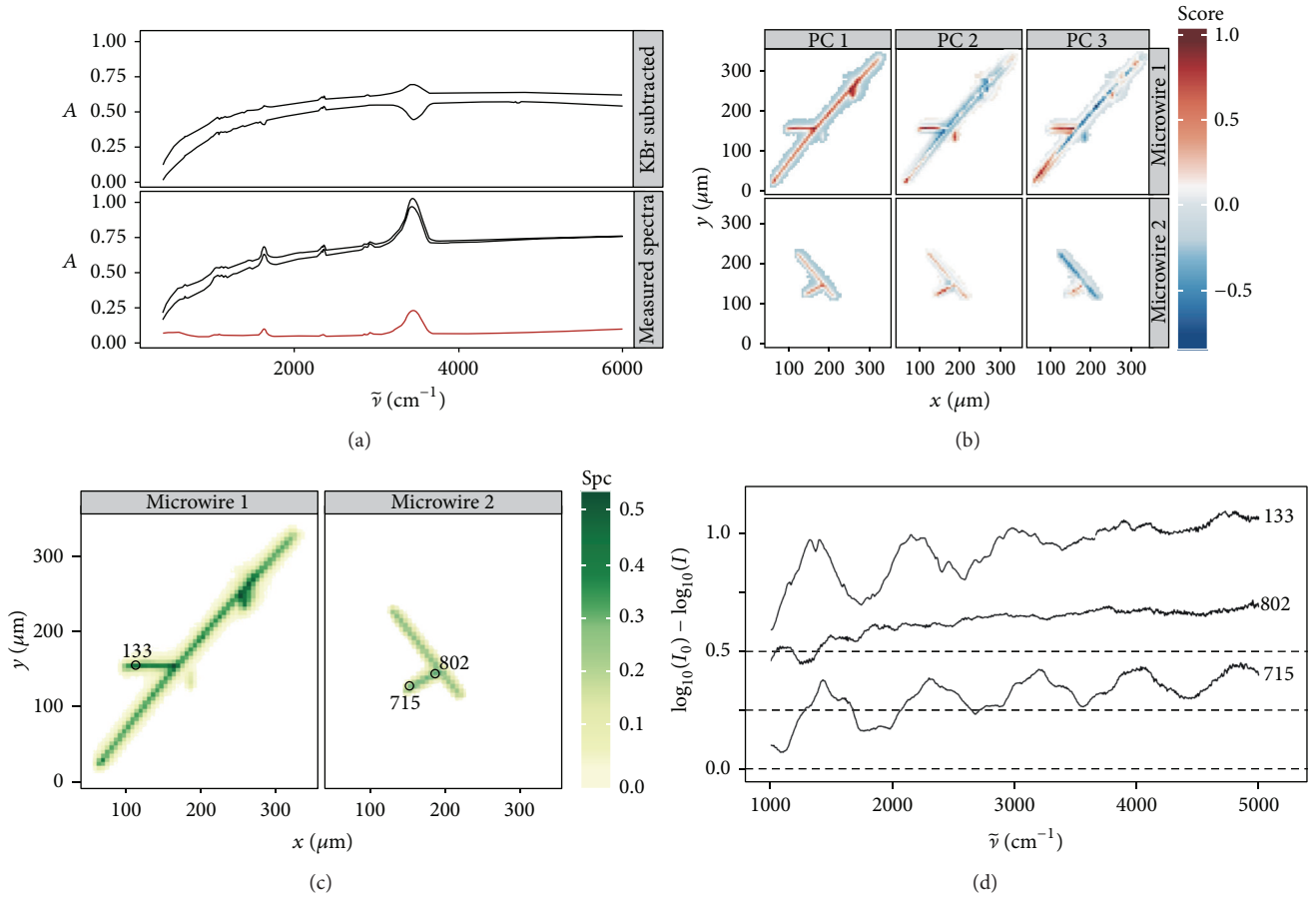

FIGURE 4: (a) FTIR spectra (absorbance) as a function of the wavenumber. Lower panel: powdered zinc phosphide microwires in KBr (black, 2 tablets) and pure KBr powder (red line). Upper panel: corrected spectra for zinc phosphide powder (2 tablets) and amplitude (A). (b) PCA scores of the microwire spectra. (c) Average absorbance map of two λ lambda-shaped microwires in the spectral range from 1000 to 5000 cm^{-1}. (d) FTIR absorbance spectra at the reference locations of (c).

radiation, which is defined as noise [49]. As the statistical fluctuations of the background photon flux incident on the detector (photon noise) increase with the detector area [50–52], the *Melanophila acuminata* adaptation for this is the small pinhole size of individual sensilla which would reduce the thermal noise [8].

Kirchhoff's law states that energy conservation is required if a body is in thermal equilibrium with its surrounding environment:

$$\phi_{\text{incident}} = \phi_{\text{absorbed}} + \phi_{\text{reflected}} + \phi_{\text{transmitted}}. \quad (2)$$

Emissivity and absorptivity go hand in hand. Thus good absorbers are good emitters and vice versa. So if an object at temperature T emits less energy than a black body at T, then it takes more energy to keep it at T because it absorbs less of what is available [51].

The noise problem in cameras and acoustical sensor systems, and also in our system, is the detection and elimination of the diverse noisy contributions from the picture-producing parts of the camera, and *M. acuminata* with his natural sensor must also overcome noise. In any sensor systems the main contributions of the noise components are white (band) noise, popcorn noise, and thermal inducted low band or spike-like noise.

A solution is given by *M. acuminata*, with its infrared sensors that contain between 150 and 200 sensilla. Each sensillum detects the spread of noise on the average value distribution [53]. Based on the averaging phenomena of the *sensilla*, it is possible to create a system using a multiple individual detectors [54, 55] to deal with equilibrium issues which can otherwise limit functionality of IR receptors.

The *M. acuminata* sensor has been modeled as a *neural network* algorithm as parallel acting average routines with different class widths, simulating retinal signal processing by neuron and ganglion structures. As in nature, these averaging signal processing structures combine different optical sensors or (small) frequency bands and therefore act as band detectors. If those band structures define the baseline signal as being clear of noise, it is possible to differentiate between noisy and nonnoisy information, that is, an increased signal to noise ratio. This is shown in Figure 5(a) which takes 91 sensors (a sensor is one unit or neurode) there by mimicking the multiple sensors of *M. acuminata* and also referred to as the auto *power* spectra [53, 56].

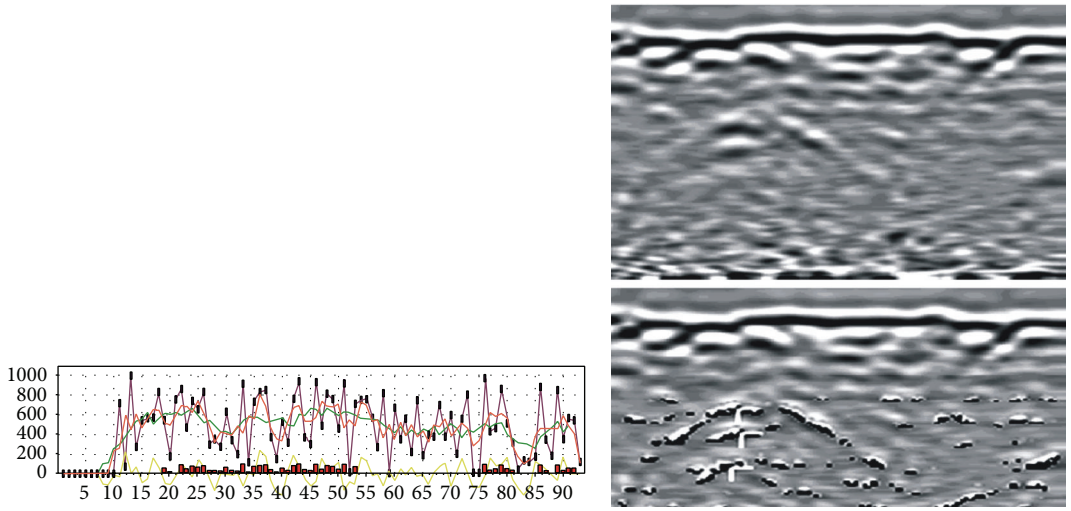

FIGURE 5: (a) Enlarging the signal-to-noise ratio by *M. acuminata*-inspired multiaveraging structures. The real signal (blue) is demodulated by a large band average (green) and a small band average (red) routine. By defining the red average line as zero line of a noise cleaned spectrum, the yellow spectrum represents the nonnoisy information spectrum, where the x-axis is the number of sensors (91 considered for this simulation) and y-axis interactions of the *neural network*. (b) Image processing by neural based self-adaptive weighting routines, for hyperbola and/or significant object detection. *Via* variable simulated receptive fields and new kinds of synaptic structures of the image processing neurons, connected subpicture structures are enhanced while other (diffuse) subpicture structures are suppressed automatically (the white triangles mark the zenith of the hyperbola).

For an optical application the algorithms implementing special neuron structures are suppressed or enlarged by self-adaptive weighting routines for local information of picture segments. Figure 5(b) shows the image processing result, done by such neuron structures on a ground penetrating *radargram*.

Zinc phosphide absorption encompasses most of the infrared spectrum [17, 57]; therefore it is an ideal material to be considered as an infrared detector. As stated in this work, the properties of Zn_3P_2 microwires, joined with the ability to use dielectrophoresis to make contacts in a branched chip structure, create the possibility that this semiconductor can be used to build infrared sensors inspired by *M. acuminata*.

7. Summary and Conclusion

Zinc phosphide photoconductivity was analysed for individual microwires in the spectral range between 425 and 1100 nm. A local maximum for the photoconductivity was found around 1000 nm of the excitation wavelength.

The FTIR spectrum of zinc phosphide microwire was compared to that from powdered zinc phosphide embedded with potassium bromide. The zinc phosphide band patterns were observed in the far infrared region, whereas the bulk spectrum in the infrared region remained unstructured (as expected from the literature), whereas the FTIR microscopic images of individual microwires reveal also their scattering properties.

In this paper we demonstrate the application of a bottom-up approach for the immobilization of an individual Zn_3P_2 nanowire in the electrode gap utilizing a sequence of dielectrophoretic manipulations for placement of Zn_3P_2 nanowires and contacting them on a preformed electrode gap.

Photoconductivity measurements were extended to the near IR range, spanning the Zn_3P_2 band gaps. Purity and integrity of the Zn_3P_2 nanowires including infrared light scattering properties were confirmed by infrared transmission microscopy.

Due to its small size microwires, on the scale of the *M. acuminata* sensilla, microwires have the advantage of overcoming photon noise which is the major limitation for the development of middle and far infrared detectors. Our experiments have successfully demonstrated that dielectrophoresis can be used for Zn_3P_2 microwire construction and conduction for the purpose of obtaining a signal from infrared radiation [55]. Based on our results, Zn_3P_2 microwires have the potential for development as a functional photoconductor in the infrared spectrum.

Conflict of Interests

Weyand Birgit, Israelowitz Meir, Henkel Thomas, Munoz Vicente,Reimers Kerstin, Vogt Peter, Gille Christoph, Rizvi Syed, Holm Christoph, and von Schroeder Herbert P. have applied for patent and gave the provisional information "Method and Apparatus related to Biomimetic-inspired Infrared Sensors," under Medical School in Hannover Germany, University of Valencia, Spain, and Institute of Photonics, Jena (no. 61821578).

Acknowledgments

The authors thank Kerdry, Lannion France, and especially Mr. Jean Claude Keromnes for his help in this project.

The authors are grateful to Dr. John E. Rawlins, Robert L. Davidson, and Robert A. Androw from the Carnegie Mellon, Museum of Natural History, Pittsburgh, PA, for providing the sample in Figure 1(a). The authors from the University of Valencia gratefully acknowledge Spanish Government and EU (FEDER) for the financial support under the Project TEC2011-28076-C02-02 and Generalitat Valenciana under the projects Prometeo/2011-035 and ISIC/2012/008, Institute of Nanotechnologies for Clean Energies of the Generalitat Valenciana. The authors thank Carolyn Connie Ferguson for the many years of moral support and wish to make a small tribute to her memory, 1933–2013.

References

[1] B. de Cock, "Qualitative and quantitative explanation of the forms of heat sensitive organs in snakes," *Acta Biotheoretica*, vol. 34, no. 2-4, pp. 193–205, 1985.

[2] E. van Hooijdonk, C. Barthou, J. P. Vigneron, and S. Berthier, "Yellow structurally modified fluorescence in the longhorn beetles *Celosterna pollinosa sulfurea* and *Phosphorus virescens* (Cerambycidae)," *Journal of Luminescence*, vol. 136, pp. 313–321, 2013.

[3] V. L. Welch, E. van Hooijdonk, N. Intrater, and J. P. Vigneron, "Fluorescence in insects," in *The Nature of Light: Light in Nature IV*, vol. 8480 of *Proceedings of SPIE*, 2012.

[4] J. J. Wolken, *Light Detectors, Photoreceptors and Imaging Systems in Nature*, Oxford University Press, 1995.

[5] T. H. Bullock and F. P. Diecke, "Properties of an infra-red receptor," *The Journal of Physiology*, vol. 134, no. 1, pp. 47–87, 1956.

[6] M. Israelowitz, S. H. W. Rizvi, and H. P. von Schroeder, "Fluorescence of the "fire-chaser" beetle *Melanophila acuminata*," *Journal of Luminescence*, vol. 126, no. 1, pp. 149–154, 2007.

[7] W. G. Evans, "Infrared radiation sensors of *Melanophila acuminata* (coleoptera: buprestidae): a thermopneumatic model," *Annals of the Entomological Society of America*, vol. 98, no. 5, pp. 738–746, 2005.

[8] M. Israelowitz, J.-A. Kwon, S. W. H. Rizvi, C. Gille, and H. P. von Schroeder, "Mechanism of infrared detection and transduction by beetle *Melanophila acuminata* in memory of Jerry Wolken," *Journal of Bionic Engineering*, vol. 8, no. 2, pp. 129–139, 2011.

[9] C. B. Anfinsen, "Principles that govern the folding of protein chains," *Science*, vol. 181, no. 4096, pp. 223–230, 1973.

[10] J. P. López-Alonso, M. Bruix, J. Font et al., "NMR spectroscopy reveals that RNase A is chiefly denatured in 40% acetic acid: implications for oligomer formation by 3D domain swapping," *Journal of the American Chemical Society*, vol. 132, no. 5, pp. 1621–1630, 2010.

[11] R. Das, P. J. Kiley, M. Segal et al., "Integration of photosynthetic protein molecular complexes in solid-state electronic devices," *Nano Letters*, vol. 4, no. 6, pp. 1079–1083, 2004.

[12] W. L. Wolfe, "Optical materials," in *The Infrared Hand Book*, vol. 7, pp. 3–128, 1978.

[13] P. L. Marasco and E. L. Dereniak, "Uncooled infrared performance," in *Infrared Technology XIX*, vol. 363 of *Proceedings of SPIE*, pp. 363–378, 1993.

[14] B. R. Frieden, *Probability, Statistical Optics and Data Testing*, Springer, New York, NY, USA, 1991.

[15] A. van der Ziel, *Noise in Solid State Devices and Circuits*, Wiley, New York, NY, USA, 1986.

[16] G. C. Holst, *Common Sense Approach to Thermal Imaging*, JCD Publishing, Winter Park, Fla, USA, 2000.

[17] R. A. Nyquist, C. L. Putzig, R. O. Kagel, and M. A. Leugers, "Infrared Spectra of Inorganic Compounds (3500–45 cm^{-1})," in *Handbook of Infrared and Raman Spectra of Inorganic Compounds and Organic Salts*, vol. 4, New York Academy Press, 1971.

[18] J. Misiewicz, "Inter-band transitions in Zn_3P_2," *Journal of Physics: Condensed Matter*, vol. 2, no. 8, pp. 2053–2072, 1990.

[19] V. V. Sobolev and N. N. Syrbu, "Optical properties and energy band structure of Zn_3P_2 and Cd_3P_2 crystals," *Physica Status Solidi B: Basic Research*, vol. 64, no. 2, pp. 423–429, 1974.

[20] P. Wu, Y. Dai, Y. Ye, Y. Yin, and L. Dai, "Fast-speed and high-gain photodetectors of individual single crystalline Zn_3P_2 nanowires," *Journal of Materials Chemistry*, vol. 21, no. 8, pp. 2563–2567, 2011.

[21] R. Yang, Y.-L. Chueh, J. R. Morber, R. Snyder, L.-J. Chou, and Z. L. Wang, "Single-crystalline branched zinc phosphide nanostructures: synthesis, properties, and optoelectronic devices," *Nano Letters*, vol. 7, no. 2, pp. 269–275, 2007.

[22] G. M. Kimball, A. M. Müller, N. S. Lewis, and H. A. Atwater, "Photoluminescence-based measurements of the energy gap and diffusion length of Zn_3P_2," *Applied Physics Letters*, vol. 95, no. 11, Article ID 112103, 2009.

[23] P. Wu, Y. Dai, Y. Ye, Y. Yin, and L. Dai, "Fast-speed and high-gain photodetectors of individual single crystalline Zn_3P_2 nanowires," *Journal of Materials Chemistry*, vol. 21, no. 8, pp. 2563–2567, 2011.

[24] G. Yu, B. Liang, H. Huang et al., "Contact printing of horizontally-aligned p-type Zn_3P_2 nanowire arrays for rigid and flexible photodetectors," *Nanotechnology*, vol. 24, no. 9, Article ID 095703, 2013.

[25] A. Wolff, C. Leiterer, A. Csaki, and W. Fritzsche, "Dielectrophoretic manipulation of DNA in microelectrode gaps for single-molecule constructs," *Frontiers in Bioscience*, vol. 13, no. 17, pp. 6834–6840, 2008.

[26] C. Leiterer, G. Broenstrup, N. Jahr et al., "Applying contact to individual silicon nanowires using a dielectrophoresis (DEP)-based technique," *Journal of Nanoparticle Research*, vol. 15, no. 5, article 1628, 2013.

[27] V. Munoz, D. Decroix, A. Chevy, and J. M. Besson, "Optical properties of zinc phosphide," *Journal of Applied Physics*, vol. 60, no. 9, pp. 3282–3288, 1986.

[28] D. Decroix, V. Muñoz, and A. Chevy, "Growth and electrical properties of Zn_3P_2 single crystals and polycrystalline ingots," *Journal of Materials Science*, vol. 22, no. 4, pp. 1265–1270, 1987.

[29] H. A. Pohl, *Dielectrophoresis: the Behaviour of Neutral Matter in Nonuniform Electric Fields*, Cambridge University Press, Cambridge, UK, 1979.

[30] H. A. Pohl and J. S. Crane, "Dielectrophoresis of cells," *Biophysical Journal*, vol. 11, no. 9, pp. 711–727, 1971.

[31] T. Schelle, T. Müller, G. Gradl, S. G. Shireley, and G. Fuhr, "Dielectrophoretic manipulation of suspended submicron particles," *Electrophoresis*, vol. 21, pp. 66–73, 2000.

[32] H. J. Keh and P. Y. Chen, "Slow motion of a droplet between two parallel plane walls," *Chemical Engineering Science*, vol. 56, no. 24, pp. 6863–6871, 2001.

[33] P. R. Griffiths and J. A. de Haseth, *Fourier Transform Infrared Spectrometry*, Wiley, 2007.

[34] J. M. Chalmers and P. R. Griffiths, *Handbook of Vibrational Spectroscopy*, Wiley, 2006.

[35] R Core Team, *R: A Language and Environment for Statistical Computing*, R Foundation for Statistical Computing, Vienna, Austria, 2012, http://www.R-project.org.

[36] C. Beleites and V. Sergo, "hyperSpec: a package to handle hyperspectral data sets in R, R package version 0. 98-201209223," 2013, http://hyperspec.r-forge.r-project.org.

[37] H. Wickham, *Ggplot2: Elegant Graphics for Data Analysis*, Springer, New York, NY, USA, 2009.

[38] E. A. Fagen, "Optical properties of Zn_3P_2," *Journal of Applied Physics*, vol. 50, no. 10, pp. 6505–6515, 1979.

[39] I. G. Stamov, N. N. Syrbu, and A. V. Dorogan, "Energetic band structure of Zn_3P_2 crystals," *Physica B: Condensed Matter*, vol. 408, no. 1, pp. 29–33, 2013.

[40] G. P. Chuiko, N. L. Don, and V. V. Ivchenko, "Ordering and polytypism in crystals," *Functional Materials*, vol. 12, pp. 454–460, 2005.

[41] J. Andrzejewski and A. Mickiewicz, "Energy band structure of Zn_3P_2-type semiconductor: analysis of the crystal structure simplification and energy band calculations," *Physica Status Solidi B*, vol. 227, pp. 515–540, 2001.

[42] D. M. Stepanchikov and G. P. Chuiko, "Excitons into one-axis crystals of zinc phosphide (Zn_3P_2)," *Condensed Matter Physics*, vol. 12, no. 2, pp. 239–248, 2009.

[43] Y. P. Varshni, "Temperature dependence of the energy gap in semiconductors," *Physica*, vol. 34, no. 1, pp. 149–157, 1967.

[44] R. Kronig and W. G. Penney, "Quantum mechanics of electrons in crystal lattices," *Proceedings of the Royal Society of London A*, vol. 130, pp. 439–531, 1930.

[45] J. R. Hook and H. E. Hall, *Solid States Physics*, John Wiley & Sons, 1991.

[46] D. A. McQuarrie, "The Kroning-Penney model: a single lecture illustrating the band structure of solids," *The Chemical Educator*, vol. 1, pp. 1–8, 1996.

[47] W. L. Wolfe, "Optical materials," in *The Infrared Hand Book*, vol. 7, pp. 3–128, 1978.

[48] G. Socrates, *Infrared and Raman Characteristic Group Frequencies: Tables and Charts*, Wiley, Chichester, UK, 2001.

[49] E. L. Dereniak and G. D. Boreman, *Infrared Detectors and Systems*, John Wiley & Sons, 1996.

[50] G. R. Pawley, *Handbook of Biological Confocal Microscopy*, Springer, 2nd edition, 1995.

[51] M. Born and E. Wolf, *Principles of Optics*, Cambridge University Press, 7th edition, 1997.

[52] W. L. Wolfe and G. J. Ziss, *Radiation Theory*, MIT PressThe Infrared Handbook, Optical Engineering Press, Bellingham, Wash, USA, 1990.

[53] M. Reuter, "Analyzing the structure of poly-crystalline materials by 2-dimensional DLS-spectra and neural nets," in *Computational Intelligence*, vol. 2206 of *Lecture Notes in Computer Science*, pp. 420–427, Springer, 2001.

[54] M. Israelowitz, S. W. H. Rizvi, C. Holm, C. Gille, and H. P. von Schroeder, "Method to detect poor infrared rays, microchip that is able to detect poor infrared rays and apparatus working with these microchips," European Union Patent EP2051303 (A2), 2007.

[55] M. Israelowitz, S. W. H. Rizvi, C. Holm, C. Gille, and H. P. von Schroeder, "Method for producing a microchip that is able to detect infrared light with a semiconductor at room temperature," USPTO 2009000141, 2009.

[56] S. Bohlmann and M. Reuter, "Supervising MultiCut aggregates by special neural nets," in *Proceedings of the World Automation Congress (WAC '12)*, Puerto Vallarta , Mexico, June 2012.

[57] R. P. Singh and S. L. Singh, "Vacuum-evaporated zinc phosphide films and their characterization," *Physica Status Solidi A*, vol. 100, pp. 493–500, 1986.